Nanoscale Advances

ROYAL SOCIETY OF CHEMISTRY

PAPER

View Article Online
View Journal | View Issue

Cite this: *Nanoscale Adv.*, 2025, **7**, 4886

Effect of the catechol structure on the functionalization and magnetic properties of barium hexaferrite nanoplatelets†

Katja Drobež, *[ab] Nina Popov‡[a] and Darja Lisjak [a]

In this study, barium hexaferrite nanoplatelets (BHF NPLs) were functionalized with different catechols, pyrocatechol (CAT), dopamine (DA), and caffeic acid (CAFA). Possible adsorption mechanisms, structural effects, and their potential impact on the functionalization and decomposition of the NPLs were investigated. We synthesized the BHF NPLs hydrothermally and functionalized them with catechols in an aqueous suspension (pH = 3) using ultrasonication or heating at 80 °C. We characterized the morphologies and size distributions of the core and functionalized BHF NPLs using transmission electron microscopy (TEM). The functionalization of the BHF NPLs was followed by electrokinetic measurements and diffuse reflectance infrared Fourier transform spectroscopy (DRIFTS). Mass fractions of ligands in the functionalized samples were determined by thermogravimetric analysis (TGA), and the room-temperature magnetic properties of the core and functionalized BHF NPLs were measured with a vibrating-sample magnetometer (VSM). The analyses showed that CAT and CAFA attached stably under the studied conditions, whereas the attachment of DA with an electron-donating group was labile. Chemical analysis of the dissolved iron ions performed with inductively coupled plasma-optical emission spectroscopy (ICP-OES) revealed that catechols enhanced the decomposition of the BHF NPLs at acidic pH.

Received 12th December 2024
Accepted 5th June 2025

DOI: 10.1039/d4na01035c

rsc.li/nanoscale-advances

1 Introduction

Barium hexaferrite (BHF), with the formula $BaFe_{12}O_{19}$, is one of the M-type hexaferrites.[1] Its applications include permanent magnets, magnetic recording, microwave devices, and absorbers.[2] Additionally, BHF nanoplatelets (NPLs) were used for developing the first ferromagnetic fluids,[3,4] alternative contrast agents for bioimaging,[5] and spin-memory devices.[6] BHF single crystals are of a hexagonal plate-like shape, and the hydrothermally synthesized nanoparticles of BHF are NPLs with a thickness of a few nanometers coinciding with the *c*-crystal axis and a larger diameter of a few tens to a few hundred nanometers along the *ab* plane.[7]

In a hexagonal unit cell of BHF Fe(III) ions occupy five characteristic crystallographic sites along the *c*-axis: a tetrahedral ($4f_1$ site), octahedral (2a, $4f_2$, and 12k sites), and trigonal bipyramidal (2b site).[8] The terminal crystal plane of the BHF NPLs is determined by the chemical environment.[9] Depending on the aqueous solution composition, whole atomic layers are removed from the NPL surfaces, changing the termination crystal plane. At basic pH with an excess of Ba (as applied during the hydrothermal synthesis), the NPLs are terminated with the crystal plane containing Ba and Fe at 2b sites. By lowering the pH of the solution (during washing with dilute nitric acid), the excess of Ba (used during the synthesis) is removed. Consequently, the 12k Fe-containing crystallographic site is the closest to the surface of the NPL and is terminated with oxygen or hydroxyl groups.[10] In our study, we used Sc^{3+}-substituted BHF NPLs because they have a significantly narrower diameter-size distribution than the unsubstituted ones.[7] The lack of large NPLs (>100 nm) enabled their colloidal stabilization in alcohols (not possible for the unsubstituted NPLs), which led to the development of ferromagnetic liquids.[3,4] A detailed crystallographic investigation confirmed the same structural pattern[11] as in the unsubstituted NPLs[10] with the 12k Fe-terminal surface plane. Considering that the Fe in BHF is only trivalent, one can expect similar surface interactions with the surrounding media for the BHF NPLs to any other Fe(III) oxide nanoparticles (*e.g.*, maghemite, hematite, or goethite).

The surface chemistry of nanoparticles is highly chemically reactive in comparison to the bulk. Due to the large surface-to-volume ratio, nanoparticles' surface chemistry significantly impacts the interactions within a given system. Consequently, one can tune the physico-chemical properties of nanoparticles through surface functionalization. One of the simple and readily exploitable approaches for metal oxide surfaces is

[a]*Department for Material Synthesis, Jožef Stefan Institute, 1000 Ljubljana, Slovenia. E-mail: katja.drobez@ijs.si*

[b]*Jožef Stefan International Postgraduate School, 1000 Ljubljana, Slovenia*

† Electronic supplementary information (ESI) available: Fig. S1–S8.† See DOI: https://doi.org/10.1039/d4na01035c

‡ Now with the Ruđer Bošković Institute, Bijenička cesta 54, 10 000 Zagreb, Croatia.

functionalization with coordinative ligands, such as catechols, carboxylic acids, and phosphonic acids.[12–14] Their functional groups (phenol, carboxyl, and phosphonic, respectively) coordinate with the surface metal ions. However, the excessive surface energy combined with strong coordinative and solvation interactions can also result in the decomposition of nanoparticles in the presence of strong complexants.[15–17] If the nanoparticles consist of toxic metals, their chemical instability becomes a critical concern, as toxic ions can be released during their use or after, *i.e.*, when disposed of in the environment. Although BHF is a chemically stable compound, its NPLs can decompose in aqueous solutions of some phosphonic acids at 80 °C.[18]

In this study, we were interested in how the BHF NPLs interact with naturally present complexants, such as catechols. Catechols efficiently functionalize iron oxide nanoparticles and even induce their decomposition.[19–21] Therefore, we assumed that they could also interact with the BHF NPLs. Catechols are abundant in nature and interact with almost all varieties of surfaces. Depending on the type of substrate, catechols can adsorb *via* various interaction mechanisms, from weak van der Waals forces to strong covalent bonds.[22] Catechol groups have a strong affinity for hydrophilic surfaces. The interaction of catechols with metallic surfaces occurs mainly through coordination bonds between the metal atoms at the surface and the catechols' phenolic groups.[22] The chemical composition of a catechol and metal oxide determines the type of surface complex.[23] Some of the possible surface complexes (Fig. 1) are outer-sphere (*i.e.*, interaction between the catechol and metal oxide surface through hydrogen bonding or van der Waals forces; Fig. 1a), while the others are mononuclear bidentate (*i.e.,* both phenolic groups of a catechol coordinate with the same metal ion on the oxide surface; Fig. 1b) and binuclear bidentate inner-sphere (*i.e.*, the ligand coordinates with two adjacent metal ions; Fig. 1c).[16,24] The bidentate binuclear coordination inhibits the dissolution of metal oxides but is not as energetically favored as mononuclear bidentate coordination that induces dissolution.[25,26] Similarly, mono- and bi-nuclear (as in Fig. 1b and c, respectively) catechol complexes were detected on the surfaces of the Fe_2O_3 and ZrO_2 nanoparticles. The high stability of the catechol surface complexes was attributed to the reconstruction of the undercoordinated surface metal sites.[19]

Additional functional groups on the catechol can affect its adsorption on metal-oxide surfaces. For example, the carboxy groups in dihydroxyphenyl acids compete to bind to metal surface sites with the phenol (*i.e.*, dihydroxyphenyl) groups.[27] Catechols with an additional electron-donating group formed more stable bidentate complexes with anatase (TiO_2) nanoparticles than those with an additional electron-withdrawing group.[28] Due to the superior stability of the Fe(III) complexes with some catechols having an electron-donating group, such as dopamine or mimosine, the decomposition of magnetite (Fe_3O_4) nanoparticles was promoted in aqueous solutions.[19]

In addition to the mentioned parameters, the solvent also affects the type and stability of the surface interaction between the catechol and metal oxide. Water is the most frequently used solvent for several reasons, *e.g.*, being an excellent environmentally friendly, and biocompatible solvent for numerous catechol structures. As catechols have a higher affinity to the surfaces than water molecules, they exchange for pre-adsorbed water molecules.[29,30] Therefore, the activation energy for adsorbing the catechol due to the energy required for desorbing water molecules from the surface before the catechol adsorption is higher than that for the adsorption of catechols on a "clean" surface. In the case of co-adsorption of catechol with water, the catechol–surface interaction energy is lower than that in the absence of water.[31] The formation of metal–catechol bonds is also influenced by the pH value in correlation with the pK_a values of catechol (Table 1). At higher pH, phenol groups deprotonate to a greater extent than at low pH values, thus promoting the catechol coordination interaction with the metal and consequently stronger cohesive forces.[22,23,32] Additional functional groups can tune the pH of deprotonation. For example, the electron-withdrawing groups (*e.g.*, carboxyl) decrease the pK_a value of the catechol phenol groups (Table 1). Consequently, increasing the medium pH >5.5 enhances the complex formation.[33]

We investigated possible surface functionalization and decomposition of the BHF NPLs with catechols having different structures (Fig. 2), a basic pyrocatechol (CAT), dopamine (DA) with an additional electron-donating amine group, and caffeic acid (CAFA) with an additional electron-withdrawing carboxyl group.

2 Experimental

2.1 Materials and methods

Iron(III) nitrate nonahydrate ($Fe(NO_3)_3 \cdot 9H_2O$, 98+ %), barium(II) nitrate ($Ba(NO_3)_2$, 99.95%), scandium(III) nitrate hydrate ($Sc(NO_3)_3 \cdot xH_2O$, 99.9%), sodium hydroxide (NaOH, 98%) and dopamine hydrochloride (99%) were purchased from Alfa Aesar. Nitric(V) acid (HNO_3, 65%) and caffeic acid were purchased from Sigma-Aldrich. Pyrocatechol (>99%) was purchased from Fluka (Switzerland). The precise metallic composition of the metal salts was determined utilizing

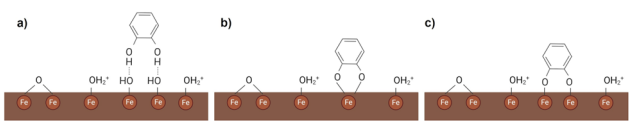

Fig. 1 Coordination interactions modes of a catechol with the Fe-oxide surface, *e.g.*, BHF NPLs in an aqueous solution at acidic pH: (a) outer and (b and c) inner sphere complex; (b) mononuclear bidentate (or chelating); (c) binuclear bidentate.

Table 1 pK_a values of catechols used correlated with the specific groups shown in Fig. 2

Catechol	pK_{a_1}	pK_{a_2}	pK_{a_3}
CAT[16]	9.4	12.8	
DA[34]	8.89	10.41	13.1
CAFA[33]	4.8	8.6	11.2

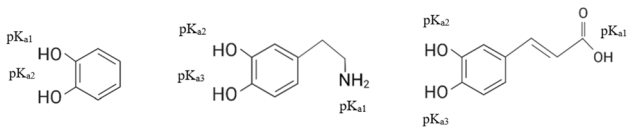

Fig. 2 Skeletal formulas, names, and abbreviations of catechols used in this study. The pK_a values are given in Table 1.

Inductively Coupled Plasma-Optical Emission Spectroscopy (ICP-OES) (Agilent 5800 ICP-OES). In all syntheses, deionized (DI) water was used.

The BHF NPLs were synthesized with a hydrothermal method in an Inconel autoclave (Parr Instrument Co.) following a well-established procedure described previously.[7] We partly substituted Fe(III) with Sc(III) for the reasons explained in the Introduction. Iron, barium, and scandium nitrates were dissolved in 400 ml of water in a molar ratio of 4.5 : 1 : 0.5. After thoroughly mixing the suspension, an excess of NaOH was added to precipitate the constituting cations from the aqueous solution. Then, the mixture was transferred into the autoclave and heated with a heating rate of 3 °C min^{-1} to 245 °C. After that, the mixture was cooled naturally to room temperature. The BHF NPLs prepared in this way were sedimented by centrifugation (Centrifuge 5804, Eppendorf), washed three times with water, to remove the unreacted reagents, and once with nitric acid at a pH 0.77, which dissolves Ba-rich compounds (*e.g.*, barium carbonate) formed as a consequence of the Ba excess. The final product was dispersed in water and treated with an ultrasonic probe (Sonics Vibra-Cell) for 1 min at 200 W. The obtained aqueous suspension of BHF NPLs had a pH of 1.65.

After that, the BHF NPLs were functionalized with catechols. For this, we used two different procedures, *i.e.*, the ultrasonic (US) and heating procedure. In both procedures, we used the aqueous suspension of the BHF NPLs, to which 250 ml of aqueous solutions of the selected catechol (Fig. 2) was added. The concentration of the catechol solutions was set to be equivalent to 2 and 10 molecules per nm^2 of NPLs. The selected nominal surface densities represent the deficiency and excess of the ligands, respectively, considering the theoretical maximum surface density, *i.e.*, 3 molecules per nm^2. An approximate surface area of the NPLs was calculated from the average size (Fig. 3b). The pH of the reaction suspension was 3. The final concentration of BHF NPLs in the reaction suspension was 0.4 mg ml^{-1}. For the US procedure, the flask containing the reaction suspension was placed in an ultrasonic bath (Sonics 4, Iskra) for 2 hours. In the heating procedure, the sonication step was substituted by heating the reaction suspension at 80 °C for 3 hours under reflux. The suspension was stirred throughout the process. The functionalized NLPs were sedimented by centrifugation (Sorvall Lynx 6000 Superspeed Centrifuge, Thermo Fisher Scientific Inc., Waltham, MA, USA) five times at 5–50.000 rcf for 5–15 min. After each centrifugation, the particles were magnetically separated from the supernatant and redispersed in DI water. In all experiments, the final (washed five times) product and the unwashed product were analyzed. The final samples and the processing conditions are listed in Table 2 while the adjective »unwashed« will be added when discussing the unwashed samples.

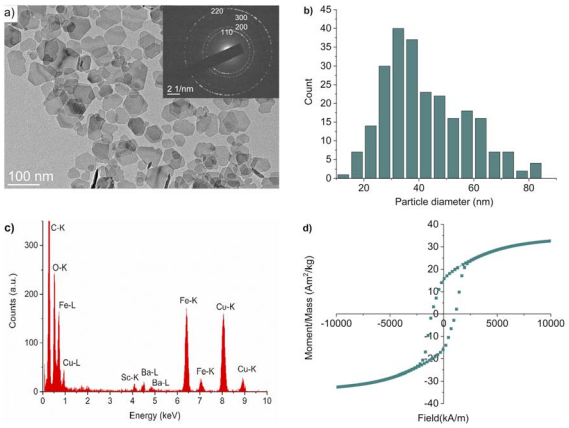

Fig. 3 The core BHF NPLs: (a) TEM image with the corresponding SAED pattern (in the inset), (b) diameter distribution, (c) EDXS spectrum, and (d) magnetization hysteresis loop. The indices in the SAED pattern correspond to the space group $P6_3/mmc$ (194).

The control sample (BHF@control) was treated using the same procedure as that for the functionalized BHF NPLs, except that no catechol was added in the reaction suspension of core NPLs.

For a comparative study, a batch of NPLs was functionalized with CAT using the US procedure at pH 10 (adjusted with ammonia solution). For this purpose, a special batch of the core BHFb NPLs was synthesized. We used the same procedure as above for the BHF NPLs. The difference was in the washing procedure. The BHFb NPLs were washed seven times only with water. The obtained suspension had a pH of 10.7. The sample was named BHFb@CAT10b.

2.2 Characterization

Several analytical methods were used to characterize the samples.

The morphologies of the as-synthesized BHF NPLs were analyzed using a transmission electron microscope (TEM, Jeol 2100) coupled with energy-dispersive X-ray spectroscopy (EDXS, JED 2300 EDS). A few drops of the diluted suspensions of BHF NPLs were deposited on a copper-supported TEM grid and left to dry. The size (*i.e.*, diameter) distributions of NPLs were determined from the equivalent diameters using DigitalMicrograph Gatan Inc. software, where 150–300 particles per sample were accounted for in statistics.

The crystal structure of dried as-synthesized BHF NPLs was also confirmed with X-ray diffraction (XRD, PANalytical X'Pert PRO). The measurement conditions were as follows: 2θ = 20–65°, step = 0.034° s^{-1}, and counting step 20 s per step.

Electrokinetic measurements were performed with a particle analyzer (Litesizer 500, Anton Paar). The zeta potentials of the core and functionalized BHF NPL suspensions were evaluated as a function of pH in 0.01 M KCl from the measured electrophoretic mobilities using the Smoluchowski model. The pH of

Table 2 List of the prepared samples with specific processing conditions. The given sample names are for the final (*i.e.*, completely washed) samples

Sample	Processing conditions
BHF@control	Control sample, US
BHF@control-80	Control sample, heating at 80 °C
BHFb@CAT10b	Functionalized with 10 mol nm^{-2} of pyrocatechol, US, pH = 10
BHF@CAT2	Functionalized with 2 mol nm^{-2} of pyrocatechol, US
BHF@CAT2-80	Functionalized with 2 mol nm^{-2} of pyrocatechol, heating at 80 °C
BHF@CAT10	Functionalized with 10 mol nm^{-2} of pyrocatechol, US
BHF@CAT10-80	Functionalized with 10 mol nm^{-2} of pyrocatechol, heating at 80 °C
BHF@DA2	Functionalized with 2 mol nm^{-2} of dopamine, US
BHF@DA2-80	Functionalized with 2 mol nm^{-2} of dopamine, heating at 80 °C
BHF@DA10	Functionalized with 10 mol nm^{-2} of dopamine, US
BHF@DA10-80	Functionalized with 10 mol nm^{-2} of dopamine, heating at 80 °C
BHF@CAFA2	Functionalized with 2 mol nm^{-2} of caffeic acid, US
BHF@CAFA2-80	Functionalized with 2 mol nm^{-2} of caffeic acid, heating at 80 °C
BHF@CAFA10	Functionalized with 10 mol nm^{-2} of caffeic acid, US
BHF@CAFA10-80	Functionalized with 10 mol nm^{-2} of caffeic acid, heating at 80 °C

the suspensions was adjusted with 0.1 M HCl and 0.1 M KOH solutions.

Diffuse Reflectance Infrared Fourier Transform Spectroscopy (DRIFTS) was used to follow the presence of ligands in the functionalized BHF NPLs. A dried ground sample (between 2 and 3 mg) was mixed with KBr (around 10 wt%) for the measurement. The absorbance was measured in a range between 4000 and 400 cm^{-1}.

Any potential dissolution of the unwashed functionalized BHF NPLs was assessed from the concentration of the dissolved iron with ICP-OES (Agilent 5800 ICP-OES), as in the NPLs there is considerably more iron than barium and scandium.[35] Besides that, scandium and barium are not present at the NPLs' terminal plane. For this purpose, we dialyzed samples' suspensions against water to separate all the NPLs from the analytical solution of the dissolved ions. Preliminary experiments showed that one-day dialysis was sufficient since the same results were obtained after one week. After that, the solution was concentrated at 80 °C, using a pressure of 100 mbar and rotation of 100 rpm with a rotary evaporator (Heidolph Hei-VAP Precision).

The mass fractions of ligands in the samples were determined by thermogravimetric analysis (TGA). A thermal analyzer (NETZSCH STA 449C/6/G Jupiter – QMS 403) was coupled with a mass spectrometer (MS). The analyses were done at a heating rate of 10 °C min^{-1} from 35 to 1000 °C in an oxidizing atmosphere, *i.e.*, in a mixture of argon and oxygen. The mass loss for the respective ligands was correlated with the temperature range of their decomposition, in particular 100–400 for CAT, 150–580 for CAFA, and 230–650 °C for DA. For the estimation of the maximum possible surface density of the ligands, we assumed that all the molecules are adsorbed on the NPL surfaces while the NPLs' surface area was calculated from an average diameter of 50 nm, an average thickness of 4 and a crystallographic density of ~5.3 g cm^{-3} (standard diffraction data no 84-0757).

The room-temperature magnetic properties of the core and functionalized NPLs were measured using vibrating-sample magnetometers LakeShore Cryotronics Series 8600 VSM and LakeShore Series 7400 VSM. A known mass of the dried ground sample (between 10 and 20 mg) was placed in a holder, tightly compressed, and placed in a uniform magnetic field of the VSM. The measurements were done in a continuous loop mode in the range between −10 kOe and 10 kOe.

3 Results and discussion

3.1 Core BHF NPLs

The core BHF NPLs (Fig. 3) are very thin, *i.e.*, approximately 3–5 nm, with an average equivalent diameter of 43 nm and a standard deviation of ± 15 nm. Their structure corresponds to that of $BaFe_{12}O_{19}$ as confirmed by selected-area electron diffraction (SAED) performed on various areas of the TEM sample and with the XRD analysis (Fig. S1†). The presence of all constituent elements was confirmed with EDXS (Fig. 3c). The cation composition measured on different NPLs slightly varies from site to site. The average composition measured on multiple batches is $Ba_{1\pm0.08}Fe_{14.9\pm0.12}Sc_{0.87\pm0.10}O_x$.[11] The magnetic hysteresis loop of core BHF NPLs confirms that they are ferrimagnetic (Fig. 3d). The BHF NPLs are a hard-magnetic material with coercivity Hc = 87 kA m^{-1}. The measured saturation magnetization, M_s, was 34 emu g^{-1}. However, considering the 0.4 wt% of nonmagnetic species (*e.g.*, nitrates and adsorbed water – see the Experimental section), the M_s of the core BHF NPLs is 38 emu g^{-1}. The fraction of the nonmagnetic species was determined thermogravimetrically (see Fig. 4).

3.2 Functionalization of the BHF NPLs

The presence of all three ligands in the functionalized samples was inferred from the thermal analyses. Exemplary TGA curves and MS spectra of the CAT-functionalized sample are shown in Fig. 4, and data for the other two samples are shown in Fig. S2.† All three ligands decomposed completely. CAT decomposed at ≤200 °C, whereas CAFA and DA decomposed at ≤600 °C.

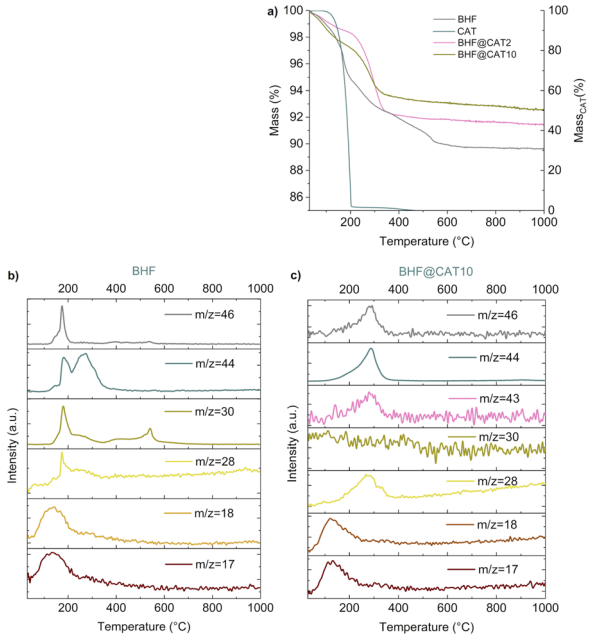

Fig. 4 Thermal analysis data: (a) TGA of the core NPLs, CAT, and BHF@CAT NPLs, (b) MS of the core NPLs, and (c) MS of BHF@CAT. In panel a, the left y-axis depicts the total mass loss of the NPLs, and the right y-axis depicts the mass loss of the ligand. The fragments in panels b and c with $m/z = 17$ correspond to OH, $m/z = 18$ to H_2O, $m/z = 28$ to CO and C_2H_4, $m/z = 30$ to NO, $m/z = 43$ to C_3H_7, $m/z = 44$ to CO_2, and $m/z = 46$ to NO_2 and CH_2O_2.

The TGA curve of the core NPLs shows three steps (Fig. 4a). The mass loss <200 °C is associated with the loss of water, carbonate, and nitrate species (Fig. 4b). An additional release of CO_2 is detected at 200–300 °C, whereas at 400–600 °C the release of NO is detected. The total mass loss of the core NPLs due to adsorbed species was 10.4% with the major mass loss associated with the decomposition of nitrates above 200 °C.

The total mass loss in the CAT-functionalized NPLs was lower than that in the core BHF NPLs, in particular, 8.5 and 7.4% for the NPLs with nominal 2 and 10 CAT molecules per nm^2, respectively. The lack of the NO (m/z = 30) fragment (Fig. 4c) suggests that the nitrates were removed during the functionalization, which was also confirmed with FTIR (Fig. 5a). The $m/z = 46$ peak is detected at a higher temperature (>200 °C) than for the core NPLs and is associated with the CH_2O_2 from CAT. In the same temperature range, we observe the carbohydrate fragments. The release of water and CO_2 fragments extends almost up to 400 °C. We can assume that they are associated, at least in part, with the decomposition of CAT. Compared to the pure compound, the higher decomposition temperature of CAT indicates its higher stability, most likely due to its attachment to the NPLs.[36]

TGA analysis of the CAFA-functionalized samples (Fig. S2a†) shows that major mass loss occurs up to 400 °C. The total mass loss of BHF@CAFA2 and BHF@CAFA10 was 8.2 and 9.1%, respectively. Similar to the CAT-functionalized samples, the NO ($m/z = 30$) fragment is also missing for the CAFA-functionalized NPLs, while the $m/z = 46$ peak can be associated with the CH_2O_2 fragment. At 200–400 °C, the release of carbohydrate fragments and CO_2 was observed, and the release of H_2O and OH fragments extended to 400 °C. Both can be correlated with the decomposition of CAFA. The minor mass loss above 400 °C can be attributed to the third decomposition step of CAFA, particularly to the carbohydrate decomposition and evaporation of CO associated with $m/z = 28$ and H_2O associated with $m/z = 18$ and 17.

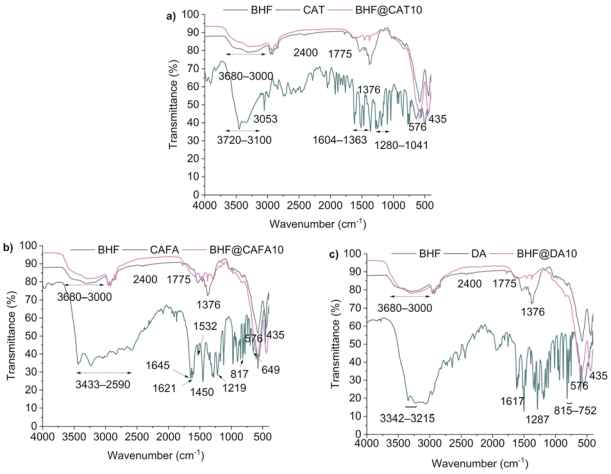

Fig. 5 DRIFT spectra of the BHF NPLs functionalized with (a) CAT, (b) CAFA, and (c) DA. The DRIFT spectra of core BHF NPLs and pure ligands are added for comparison.

The total mass losses of the functionalized NPLs with DA were 4.6 and 10.1% for the nominal 2 and 10 molecules of DA per nm^2, respectively (Fig. S2b†). Major mass loss in the functionalized samples occurred below 400 °C. In the corresponding MS, we observe typical DA decomposition fragments, *i.e.*, carbohydrates (m/z = 28 and 43), CO_2 (m/z = 44), H_2O (m/z = 18), and NH_3 and/or OH ($m/z = 17$) up to 400 °C. From the TGA and MS spectra, it is impossible to distinguish precisely between the nitrate residue and DA. Only a small peak associated with the NO ($m/z = 30$) fragment observed above 400 °C for BHF@DA10 indicates the possible presence of nitrates in this sample. This suggests that the nitrates were not removed (completely) as from the BHF@CAT/CAFA samples. Therefore, we could not determine what part of the total mass loss is associated with the decomposition of DA in the BHF@DA NPLs.

Additional evidence of the catechol ligands in the functionalized samples was obtained from IR spectroscopy (Fig. 5). The core BHF NPLs show a broad band between 3680 and 3000 cm^{-1} corresponding to the physisorbed and/or hydrogen-bonded water, weak bands at 2400 and 1775 cm^{-1} corresponding to the carbonate, a medium band at 1376 cm^{-1} corresponding to the nitrate, and two bands between 576 and 435 cm^{-1} corresponding to the tetrahedral and octahedral Fe–O vibrations.[18,37,38] The visible characteristic peaks of CAT (Fig. 5a) are at 3720–3100 cm^{-1} for OH groups, 3053 and 1280–1041 cm^{-1} for =CH, and 1604–1363 cm^{-1} for C=C of a benzene ring.[37]

The DRIFT spectrum of CAT-functionalized NPLs significantly differs from the spectrum of pure CAT. It is more similar to the spectrum of core NPLs but with some distinct differences.

In the DRIFT spectrum of CAT-functionalized NPLs, the nitrate band (1376 cm^{-1}) was not observed, suggesting that nitrate was (completely) removed during the functionalization and subsequent washing. Also, the peaks of carbonate at 2400 and 1775 cm^{-1} were not observed anymore, meaning that CAT removed or exchanged it. Vibrations of the hydroxy groups (3680–3000 cm^{-1}) were not affected by the presence of CAT and can be associated with the CAT phenol groups. A band between 1374 and 1255 can be associated with the aryl–oxygen–Fe (C–O–Fe) vibration, suggesting surface complexation through the hydroxy groups at the oxide surface. A visible broad band between 1667 and 1522 cm^{-1} can be associated with the vibration of the aromatic ring of CAT.[28,39]

Typical bands observed in the CAFA spectrum (Fig. 5b) are 3433–2590 cm^{-1} for OH, 1645 cm^{-1} for C=O,[37,40] 1621, 1532, and 1450 cm^{-1} for aromatic and olefinic C–C, and 1281 and 1219 for olefinic and aromatic C–H bonds. Frequencies observed at <1121 cm^{-1} are for C–C–C bending modes of the aromatic ring, except for the frequencies at 817 and 649 cm^{-1}, which are for the carbonyl group.[41,42] Among these, the 1118 and 808 cm^{-1} peaks are also observed in the spectrum of the BHF@CAFA NPLs. The nitrates were exchanged by CAFA, similar to the BHF@CAT sample.

Typical bands observed in the DA spectrum are at 3342–3215, 1617, and 815–752 cm^{-1} for N–H, and 1287 cm^{-1} for olefinic and aromatic C–H bonds.[37,41–44] In the spectrum of BHF@DA10, peaks were observed at 1163, 1102, 1050, and 839 cm^{-1}, which can be assigned to C–O–Fe vibrations.[28] The nitrate band at 1376 cm^{-1} has low intensity. Therefore, we cannot surely say if nitrates were (completely) removed during the functionalization with DA or not.

Although the TGA, MS, and DRIFTS confirm the presence of ligands in the functionalized NPLs, none of the methods distinguishes between the adsorbed and dissolved ligand' molecules in the aqueous suspension. Therefore, we assessed the potential adsorption of ligands on the NPLs from the zeta-potential *vs.* pH behavior. We compared the washed and unwashed functionalized NPLs dispersed in water with the aqueous suspension of core BHF NPLs (Fig. 6). The core BHF NPLs had a large positive zeta potential at low pH < 6 and a large negative zeta potential at pH > 8, with the point of zero charge (PZC) at a pH of around 7.8. For the functionalized NPLs, a shift in the PZC was observed to a lower pH. The PZC of the NPLs functionalized with CAT (pH ~6) and CAFA (pH ~4) was similar for the unwashed and washed samples, suggesting a stable attachment of the ligands without significant desorption during the washing step. Similar results were obtained when using a lower nominal fraction of the ligand (Fig. S3a and b†), indicating that using an excessive ligand fraction (*i.e.*, 10 molecules per nm^2) did not significantly improve the adsorption of CAT on the NPLs.

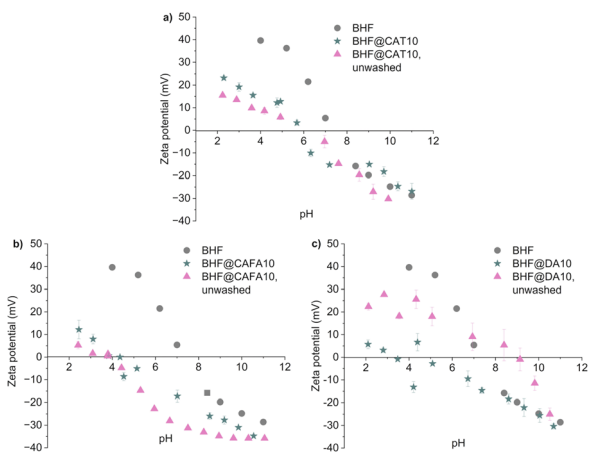

Fig. 6 Zeta potential behavior of the NPLs functionalized with the US method with a nominal surface density of 10 molecules per nm^2 of the ligands: (a) CAT, (b) CAFA, and (c) DA. For comparison, data are also given for the core BHF NPLs. Error bars denote the standard deviation of a measured point.

A significant change in the zeta-potential behavior considering the core NPLs suggests that CAT was adsorbed at the NPL surfaces *via* its phenol groups.[22,24] A decrease in the PZC from pH ~7.5 to pH ~6 was also previously observed for the maghemite nanoparticles and TiO_2 surfaces.[20,24] For the TiO_2 surface, this was attributed to the surface coordination of CAT, which enhanced the acidity of catechol.[24]

The pH of the PZC of the BHF@CAFA sample coincides with the deprotonation of the CAFA's carboxyl group,[33] suggesting that CAFA was attached to the NPLs' surfaces *via* phenolic groups. Similar PZC values were determined previously on the maghemite nanoparticles that were functionalized with CAFA at different pH values.[20,45] It seems like the pH value of the functionalization process did not influence the interaction mode of the NPLs with CAFA. In both cases, CAFA bonded with the phenolic group(s).

The maximum possible surface density of CAT, determined from the mass loss associated with the decomposition of CAT at 100–400 °C (Fig. 4a), is ~1–1.5 CAT molecules per nm^2. The actual surface density of adsorbed CAT is probably lower than the calculated value due to the dynamic equilibrium between adsorbed and desorbed ligand molecules (*i.e.*, typical for non-covalently bonded adsorbents) and must be similar for both nominal fractions, as indicated by the similar zeta-potential behaviors. Higher maximum possible surface densities, *i.e.*, ~3–3.5 CAT per nm^2, were achieved previously at functionalized maghemite NPs.[20] Apart from the different chemical composition, structure, and shape of the core particles, the functionalization pH = 8 or 11 in the previous case was higher than that in our study (*i.e.*, pH = 3). At pH > 4.8, one of the phenol groups of the CAT is deprotonated (Table 1). Therefore, it can bind electrostatically with the Fe–OH_2^+ (Fig. 1 and 6) on the surface, which seems to promote the adsorption of CAT on iron oxide surfaces. Another study[24] on the TiO_2 surface showed a remarkable decrease in CAT adsorption above pH ~8.5. Unfortunately, we could not functionalize the BHF NPLs at pH ~6–9 without agglomerating them (Fig. 6). Therefore, we prepared another batch of core NPLs, *i.e.*, BHFb NPLs, that were dispersed in water at a basic pH ~10.

The BHFb NPLs (Fig. S4†) were similar to the BHF NPLs. The only difference resulted from different washing procedures (see Experimental). Since the BHFb NPLs were not washed with the

nitric acid solution, the side synthesis product, $BaCO_3$, was not removed. $BaCO_3$ is stable and starts to decompose at high temperatures. The associated mass loss due to the evaporation of CO_2 from $BaCO_3$ was observed at ≥800 °C (Fig. S5†). The TGA curve and MS spectra of the BHFb@CAT10 NPLs (Fig. S5a and c†) were similar to those of BHF@CAT10, indicating that $BaCO_3$ dissolved during the functionalization process and the dissolved ions were removed during the washing. The maximum achieved surface density of CAT in BHFb@CAT10 (1.3 molecules per nm^2) was similar to that in BHF@CAT10 (1.2 molecules per nm^2), which was also in line with the similar zeta-potential behaviors (Fig. 6a and S6†).

When the functionalization with CAT was carried out at acidic pH = 3, CAT was fully protonated (Table 1), while the BHF NPLs have a positive surface charge due to the protonated surface hydroxyl groups (–Fe–OH_2^+; see Fig. 1 and 6). Under such conditions, only the hydrogen-bond interaction between the phenol and surface hydroxyl groups enables physisorption, which competes with the hydration interaction between the CAT and water molecules.

$$\mathrm{HO-CAT-OH(aq)+NPL-Fe-OH_2^+}(s) \overset{\mathrm{HNO_3(aq)}}{\Leftrightarrow} \mathrm{NPL-Fe-OH_2^+\cdots\ HO-CAT-OH(s)} \quad (1)$$

Alternatively, the bonded molecules could be chemisorbed after the condensation of the CAT phenol groups with the surface hydroxyl groups.

$$\mathrm{HO-CAT-OH(aq)+NPL-Fe-OH_2^+(s)+NO_3^-(aq)} \overset{\mathrm{H_2O}}{\Leftrightarrow} \mathrm{NPL-Fe-O-CAT-OH(s)+H_2O(l)+HNO_3(aq)} \quad (2)$$

Due to the lack of protons, the condensation reaction is not possible at a basic pH = 10 used for functionalizing the BHFb NPLs. The surface hydroxyl groups are deprotonated (–Fe–O^-, see Fig. 1 and S6†), and CAT is also partly deprotonated (Table 1). Therefore, CAT can only physisorb onto NPLs, *e.g.*, *via* a hydrogen bond.

$$\mathrm{HO-CAT-O^-(aq)+NPL-Fe-O^-(s)} \overset{\mathrm{H_2O}}{\Leftrightarrow} \mathrm{NPL-Fe-O^-\cdots HO-CAT-O^-(s)} \quad (3)$$

The surface condensation reaction (such as eqn (2)) is promoted at elevated temperatures.[46] Therefore, the third experiment was carried out at 80 °C while keeping the pH = 3 to ensure protons for the reaction. However, no noticeable effect of the elevated temperature was observed. The zeta-potential behavior was similar to that of the functionalized BHF NPLs prepared at room temperature (Fig. S3a†), suggesting a similar surface density of CAT in both samples. Overall, we can conclude that CAT physisorbs onto the BHF NPLs at a surface density of ≤1 molecules per nm^2 when functionalized in an aqueous suspension at acidic or alkaline pH.

The surface of BHF NPLs predominantly terminates with Fe–O(H),[9,11] similar to any other iron oxide. It is reasonable to assume that the ligands preferentially adsorb on the hydroxylated surface sites. However, it is possible that some surface metal sites are not hydroxylated (Fig. 1) since the PZC of core BHF NPLs (Fig. 6a) is more similar to that of hematite (α-Fe_2O_3) at pH 7–8 [47,48] than to that of goethite (α-FeO(OH)) at pH ∼9.[49,50] Although a higher fraction of the hydroxylated surface sites is expected for the BHFb NPLs (pH_{PZC} ∼8, Fig. S6†), the electrostatic repulsion between the negative surface and partly deprotonated CAT (eqn (3)) hinders the adsorption of CAT at basic pH ∼11.

Our results do not show any significant qualitative effect of the electron-withdrawing carboxyl group on the adsorption of catechols on the BHF NPLs at pH = 3. The zeta-potential behaviors (Fig. 6a and b) confirm stable adsorption of both ligands. The maximum possible (if all molecules are adsorbed) achieved surface density of CAFA (Fig. S2a and c†), *i.e.*, ∼1 molecule per nm^2, was similar (considering the assessment procedure) to that of the CAT-functionalized samples.[20] However, there is some difference in the decomposition of the two ligands. The pure CAT decomposes completely up to 200 °C, whereas the adsorbed CAT in the functionalized samples decomposes up to 400 °C (Fig. 4). In contrast to this, the decomposition temperature of the pure CAFA and adsorbed CAFA is similar (Fig. S2a and c†). Consequently, the adsorption energy of CAT may be higher than that of CAFA.

In contrast to the above, the surface functionalization of the NPLs with DA was not stable, considering the different zeta-potential behaviors of the unwashed and washed samples (Fig. 6c and S3c†). A shift of the PZC to a higher pH = 9 was observed for the unwashed functionalized NPLs when compared to the core NPLs with PZC at pH ∼8. However, after washing the DA-functionalized samples, the zeta potential changed significantly, and the PZC shifted to pH ∼3–5. Similar results were obtained regardless of the functionalization method, the US procedure or heating at 80 °C, and the ligand's nominal fraction, 2 or 10 molecules per nm^2.

We functionalized the BHF NPLs with DA under acidic conditions to avoid its polycondensation that occurs at basic pH.[51] DA is fully protonated at pH 3 (Table 1), and the protonated amine group (NH_3^+) is electrostatically repelled by the positively charged surface of the BHF NPLs (–Fe–OH_2^+). Therefore, we expected DA to interact with the NPLs' surface *via* its phenolic groups, while the amine group should determine the zeta potential of the functionalized NPLs. Consequently, the DA-functionalized BHF NPLs should have PZC at pH > 8 (Table 1), as was the case for the unwashed sample. Although DA adsorbed onto the surface of the BHF NPLs in the first place, it should have desorbed to a great extent during the washing.

To elucidate the conditions for the desorption of DA from the NPLs, we studied the colloidal properties of an exemplary DA-functionalized sample, BHF@DA2-80, in the long term. The PZCs of all unwashed samples were at pH value 9, and the PZCs of all the washed samples were at pH between 5 and 6 (Fig. S7†). The time of exposure to solvent (DI water) did not affect the colloidal properties of functionalized particles. The difference

between unwashed and washed samples remains the same, which means that DA desorbs because of the dilution with water; the reaction in eqn (1) is directed to the left-hand side if DA replaces CAT. The system is kinetically stable if the system's properties are kept constant (*e.g.*, no dilution).

Based on the above, we can conclude that the additional electron-donating group, *i.e.*, amine in DA, did not promote surface functionalization of the BHF NPLs compared to CAT. In contrast, the interaction of DA with the BHF NPLs at pH = 3 was labile, and the primarily adsorbed molecules were desorbed after diluting the suspension with water. The observed stability of the polydopamine coatings on other nanoparticles[51,52] can be attributed to the polycondensation of DA and not to its interaction with the metal-oxide surfaces.

The mass fractions of catechols in our samples were lower than those reported for the other iron oxide nanoparticles.[20,45,52] Note that none of the studies distinguished between the adsorbed and dissolved functionalizing ligands. The observed differences cannot be explained, in general, by different functionalization conditions or the size but by the shape effect. The iron oxide nanoparticles are quasi-spherical with a larger curvature, making them more reactive than the flat platelets, such as BHF NPLs.[53,54] In addition, steric hindrance between the surface ligands can be suppressed by a curvy surface, facilitating higher surface densities than on the flat NPL surface.

3.3 Chemical stability and magnetic properties of the functionalized BHF NPLs

A consequence of the high reactivity of some iron oxide nanoparticles was (partial) dissolution or decomposition triggered by catechols.[16,21,55] The chemical stability against the decomposition *via* dissolution was evaluated by following the fraction of dissolved Fe ions with ICP–OES of the unwashed functionalized BHF NPLs (Table 3). The concentration of the dissolved Fe was above the detection limit, indicating an onset of the decomposition of the NPLs. We compare the results relative to the dry-weight basis (DW). All samples were several months old, but there was no correlation between their age and the Fe loss. The relative loss of Fe (see atomic ratios Fe : Ba and Fe : Sc in the treated samples) was the lowest for the BHF@CAT samples and the highest for BHF@CAFA10. Despite the labile attachment of DA onto the NPLs, the Fe loss was (slightly) larger than that for the BHF@CAT samples.

We also performed a control experiment to verify whether the BHF NPLs can dissolve in the nitric acid solution. For this purpose, the core BHF NPLs were treated similarly to that during the functionalization method but without adding a ligand, *i.e.*, the control sample. In this case, the additional loss of Fe was detected, but it was significantly lower than that in the presence of catechols. Although the Fe-12k terminal plane is supposed to be stable at acidic pH applied during the surface functionalization,[9] the additional energy provided with the US treatment suffices to start the decomposition of BHF NPLs. In contrast, the sample that was kept all the time under basic conditions, *i.e.*, BHFb@CAT10b, was the most chemically stable. We can conclude that the dissolution of the BHF NPLs is initiated by protons (*i.e.*, in acidic aqueous solutions) and accelerated in the presence of catechols.

An additional assessment of a possible partial decomposition/dissolution can be obtained from the M_s values.[56] In particular, a decrease in the M_s is expected if the 12k Fe(III) ions are removed from the surface.[56] Note that only the Fe(III) ions carry a magnetic moment and that the Ba(II) and Sc(III) ions are not present in the terminal surface plane. The M_s values of the magnetic phase (Table 4) were calculated considering only the mass fraction of the core BHF NPLs, which was obtained by subtracting the mass fraction of nonmagnetic phases determined from the TGA (Fig. 4a and S2†). The M_s values of BHF@DA differ less than 10% from that of the core BHF NPLs, *i.e.*, +1% BHF@DA2 and −8% BHF@DA10, whereas the M_s of BHF NPLs functionalized with CAT and CAFA increased more than 10% in comparison to the core NPLs. Such an increase in the M_s of the core BHF NPLs contradicts the decomposition indicated by the dissolution analysis (Table 3). However, the relative Fe loss considering the NPL composition (see the Fe : Ba atomic ratio in Table 3) was insignificant, implying an insignificant effect on the M_s values.

Since the M_s of nanoparticles decreases with the decreasing size due to the increased surface spin canting,[57] we compared the diameter-size distributions of the core and functionalized NPLs (Fig. 7). The M_s values of the BHF NPLs are affected mainly by the variation of their thicknesses due to the relatively large *c*-

Table 3 The concentration of dissolved iron (γ_{Fe}) and calculated concentration on a dry weight (DW) of the core, control, and unwashed functionalized BHF NPL samples. The atomic ratios of Fe : Ba and Fe : Sc in the treated NPLs are given in the right two columns. All listed samples were prepared with the US method

Sample	Sample age [months]	γ_{Fe} [μg ml^{-1}]	DW [μg mg^{-1}]	Fe : Ba	Fe : Sc
BHF	6	0.2 ± 0.05	0.25 ± 0.06	14.89 ± 0.01	17.12
BHF control sample, unwashed	12	1.1 ± 0.05	1.31 ± 0.06	14.87 ± 0.03	17.09
BHF@CAT2, unwashed	6	0.46 ± 0.05	5.11 ± 0.56	14.77 ± 0.11	16.98
BHF@CAT10, unwashed	3	1.2 ± 0.1	8.00 ± 0.67	14.70 ± 0.18	16.90
BHFb@CAT10b, unwashed	5.5	0.041 ± 0.002	0.21 ± 0.01	14.90 ± 0.005	17.12
BHF@DA2, unwashed	6.5	2.9 ± 0.1	12.61 ± 0.43	14.58 ± 0.31	16.76
BHF@DA10, unwashed	4.5	1.9 ± 0.1	9.5 ± 0.5	14.66 ± 0.23	16.85
BHF@CAFA2, unwashed	6.5	0.99 ± 0.05	12.38 ± 0.63	14.59 ± 0.30	16.77
BHF@CAFA10, unwashed	4.5	2.5 ± 0.1	20.83 ± 0.83	14.38 ± 0.50	16.52

Table 4 Mass fractions of nonmagnetic phases, the measured and actual saturation magnetization values (M_s) of the core and functionalized BHF NPLs, and the relative deviation from the expected M_s. The experimental error of the M_s is ±0.2. The listed samples were prepared with the US method with nominal 2 and 10 mol. of ligands per nm^2

Sample	Nonmagnetic phase [wt%]	Measured M_s [A m^2 kg^{-1}]	Ms magnetic phase [A m^2 kg^{-1}]	Deviation from the expected M_s [%]
BHF	10.4	34.3	37.9	
BHF@CAT2	8.5	44.1	47.8	+26.1
BHF@CAT10	7.4	40.8	43.8	+15.6
BHFb@CAT10b	6.8	35.9	38.3	+1.1
BHF@DA2	4.6	36.6	38.3	+1.1
BHF@DA10	10.1	31.6	34.8	−8.2
BHF@CAFA2	8.2	44.1	47.7	+25.9
BHF@CAFA10	9.1	39.0	42.5	+12.1

unit-cell parameter (~2.5 nm). In contrast, their diameter is associated with much smaller (~0.6 nm) *a* and *b* parameters. Most of the NPLs with diameters between 30 and 300 nm have a thickness of 4.1 nm, and their M_s values are not significantly affected by the diameter distribution.[11] In our case, functionalization with subsequent washing and centrifugation resulted in a higher fraction of the NPLs with diameters ≤30 nm and a lower fraction of the NPLs with diameters >90 nm, which should have the opposite (if any) effect, *i.e.*, a decrease in the M_s. We also did not observe any significant changes in the thicknesses of the BHF NPLs after the functionalization. In line with this, the coercivity of the NPLs, which could be affected by the change in the NPL size, did not change significantly after the functionalization (Fig. S8†). We can conclude that the observed variation of the NPL size distribution due to the functionalization process did not contribute to an increase in the M_s values.

Considering the above, the only possible reason for the unexpectedly large increase in the M_s is an improvement in the spin colinearity at the BHF NPL surfaces provided by the coordinating catechol ligands around the surface Fe ions.[21,58,59] The distortion of the Fe(III) crystal field on the surface relative to the one in the crystal core is supposed to be smaller for the surface terminating with catechols than with O or OH. The M_s increase was measured only for the CAT- and CAFA-functionalized BHF NPLs for which the adsorption of the ligands was inferred from the zeta-potential behaviors. Oppositely, the zeta-potential behavior of the DA-functionalized NPLs did not confirm its stable attachment under the studied conditions, which is associated with a slight variation (even a decrease) of the M_s.

A similar increase in the M_s values of BHF@CAT and BHF@CAFA indicates no significant effect of the electron-withdrawing group (*i.e.*, carboxyl in CAFA) on the adsorption of catechols under given conditions. In contrast to CAT and CAFA, the electron-donating group (*i.e.*, amine in DA) had a negative effect, and DA did not adsorb robustly on the BHF NPLs at acidic pH. Moreover, an 8% decrease in the M_s of BHF@DA10 can be a consequence of a relatively high Fe loss (Table 3) that can form a soluble complex with DA that does not adsorb on the NPLs and, consequently, cannot reduce the surface spin canting as CAT and CAFA.

Interestingly, the M_s of BHFb@CAT10b did not change significantly with respect to the core NPLs (Table 4), which coincides with its superior chemical stability (Table 3).

However, its zeta-potential behavior (Fig. S5b†) was similar to that of BHF@CAT10 (Fig. 6), and the maximum achieved surface density is also comparable between the two samples. The only difference can be the mode of adsorption. While the condensation reaction (eqn (2)) is possible at acidic pH, this is not so at basic pH (eqn (3)). Therefore, CAT could only physisorb *via* a hydrogen-bond interaction on the NPLs at the basic pH.

From the other perspective, if the size effect can be excluded, an increase in the M_s of magnetic nanoparticles could be used to distinguish between the chemi- and physisorption. Most analyses, *e.g.*, TGA or different spectroscopies, do not differentiate between the adsorbed and dissolved ligands. The mass fraction of a ligand determined with TGA does not mean that the whole fraction is adsorbed on the particles' surfaces, and the detected catechol bands with FTIR do not provide direct (without comparison with the calculated spectrum) information on the ligand's interaction with a surface. The zeta-potential behavior can be applied to assess the changes of a surface charge but cannot be used in nonpolar systems. In this view, a possibility to, at least qualitatively, assess potential adsorption of ligands on the magnetic nanoparticles from the M_s values

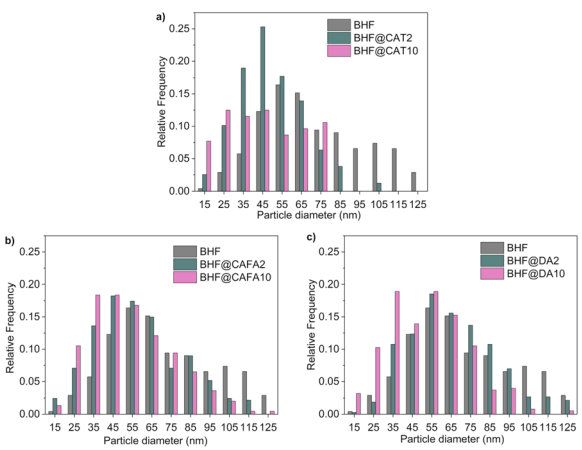

Fig. 7 Diameter-size distributions of the NPLs functionalized with nominal 2 and 10 molecules per nm^2: (a) CAT, (b) CAFA, and (c) DA. For comparison, data for the core NPLs are added.

would be valuable. However, more systematic studies beyond the scope of this contribution are needed to verify such a method.

4 Conclusions

We investigated the functionalization of barium hexaferrite nanoplatelets (BHF NPLs) with catechol-based ligands, including pyrocatechol (CAT), dopamine (DA) with an additional electron-donating amine group, and caffeic acid (CAFA) with an additional electron-withdrawing carboxyl group, under acidic conditions (pH = 3). Our findings suggest that electron-withdrawing or electron-donating groups did not enhance the adsorption of catechols under acidic conditions. In contrast, the adsorption of DA was labile, while no significant difference was observed between CAT and CAFA. Furthermore, the functionalization of NPLs was not influenced by the applied procedure of functionalization and the initial nominal densities of ligands. As a consequence of the functionalization, a minor (*i.e.*, at the limit of significance) relative loss of Fe was detected. Considering milder environmental conditions compared to those in our study, we do not expect any substantial decomposition of the disposed BHF NPLs in the presence of natural catechols. The saturation magnetization (M_s) significantly increased for the CAT- and CAFA-functionalized NPLs compared to the core BHF NPLs and was attributed to improved spin collinearity at the NPL surface by the coordinating catechols.

Data availability

The Data obtained from the magnetic, thermogravimetric, and spectroscopic measurements are available at the following link: **https://zenodo.org/records/15601820**.

Author contributions

The manuscript was written with the contributions of all authors. They all approved the final version of the manuscript.

Conflicts of interest

There are no conflicts to declare.

Acknowledgements

The authors acknowledge financial support from the Slovenian Research and Innovation Agency (ARIS) within the research core funding P2-0089 and the research projects PR-12336 and J2-2495. We also acknowledge the CEMM Nanocenter for the use of the VSM and TEM. Furthermore, the authors would like to thank Jošt Tručl for measuring the magnetic properties of the samples.

References

1 J. Smit and H. P. J. Wijn, *Ferrites*, 1959.
2 R. C. Pullar, *Prog. Mater. Sci.*, 2012, **57**, 1191–1334.
3 A. Mertelj, D. Lisjak, M. Drofenik and M. Čopič, *Nature*, 2013, **504**, 237–241.
4 M. Shuai, A. Klittnick, Y. Shen, G. P. Smith, M. R. Tuchband, C. Zhu, R. G. Petschek, A. Mertelj, D. Lisjak, M. Čopič, J. E. Maclennan, M. A. Glaser and N. A. Clark, *Nat. Commun.*, 2016, **7**, 10384.
5 J. Hu, T. Gorsak, E. Martín Rodríguez, D. Calle, T. Muñoz-Ortiz, D. Jaque, N. Fernández, L. Cussó, F. Rivero, R. Aguilar Torres, J. García Solé, A. Mertelj, D. Makovec, M. Desco, D. Lisjak, F. Alfonso, F. Sanz-Rodríguez and D. H. Ortgies, *ChemPhotoChem*, 2019, **3**, 529–539.
6 G. Koplovitz, D. Primc, O. Ben Dor, S. Yochelis, D. Rotem, D. Porath and Y. Paltiel, *Adv. Mater.*, 2017, **29**, 1606748.
7 D. Lisjak and M. Drofenik, *Cryst. Growth Des.*, 2012, **12**, 5174–5179.
8 E. Pollert, *Prog. Cryst. Growth Charact.*, 1986, **11**, 263–323.
9 M. Poberžnik, G. Herrero-Saboya, D. Makovec, D. Lisjak and L. Martin-Samos, *Appl. Surf. Sci.*, 2023, **637**, 157890.
10 D. Makovec, B. Belec, T. Goršak, D. Lisjak, M. Komelj, G. Dražić and S. Gyergyek, *Nanoscale*, 2018, **10**, 14480–14491.
11 D. Makovec, M. Komelj, G. Dražić, B. Belec, T. Goršak, S. Gyergyek and D. Lisjak, *Acta Mater.*, 2019, **172**, 84–91.
12 M. A. Neouze and U. Schubert, *Monatsh. Chem.*, 2008, **139**, 183–195.
13 C. Queffélec, M. Petit, P. Janvier, D. A. Knight and B. Bujoli, *Chem. Rev.*, 2012, 3777–3807.
14 L. Deblock, E. Goossens, R. Pokratath, K. De Buysser and J. De Roo, *JACS Au*, 2022, **2**, 711–722.
15 D. Lisjak, O. Plohl, J. Vidmar, B. Majaron and M. Ponikvar-Svet, *Langmuir*, 2016, **32**, 8222–8229.
16 H. Gulley-Stahl, P. A. Hogan, W. L. Schmidt, S. J. Wall, A. Buhrlage and H. A. Bullen, *Environ. Sci. Technol.*, 2010, **44**, 4116–4121.
17 M. Shailaja and S. V. Narasimhan, *J. Nucl. Sci. Technol.*, 1991, 1107–1114.
18 D. Lisjak, P. Hribar Boštjančič, P. Hribar Boštjančič, A. Mertelj, A. Mavrič, A. Mavrič, M. Valant, M. Valant, J. Kovač, H. Hudelja, H. Hudelja, A. Kocjan and D. Makovec, *ACS Omega*, 2020, **5**, 14086–14095.
19 M. D. Shultz, J. Ulises Reveles, S. N. Khanna and E. E. Carpenter, *J. Am. Chem. Soc.*, 2007, **129**, 2482–2487.
20 S. Čampelj, M. Pobrežnik, T. Landovsky, J. Kovač, L. Martin-Samos, V. Hamplova and D. Lisjak, *Nanomaterials*, 2023, **13**, 1822.
21 A. K. L. Yuen, G. A. Hutton, A. F. Masters and T. Maschmeyer, *Dalton Trans.*, 2012, **41**, 2545–2559.
22 J. Saiz-Poseu, J. Mancebo-Aracil, F. Nador, F. Busqué and D. Ruiz-Molina, *Angew. Chem.*, 2019, **131**, 706–725.
23 K. V. Korpany, D. D. Majewski, C. T. Chiu, S. N. Cross and A. S. Blum, *Langmuir*, 2017, **33**, 3000–3013.
24 R. Rodriguez, R. Rodriguez, M. A. Blesa and A. E. Regazzoni, *J. Colloid Interface Sci.*, 1996, **177**, 122–131.
25 W. Stumm, *Colloids Surf., A*, 1997, **120**, 143–166.
26 B. Nowack and L. Sigg, *Geochim. Cosmochim. Acta*, 1997, **61**, 951–963.

27 K. V. Korpany, C. Mottillo, J. Bachelder, S. N. Cross, P. Dong, S. Trudel, T. Friščić and A. S. Blum, *Chem. Commun.*, 2016, **52**, 3054–3057.
28 T. D. Savić, M. I. Čomor, J. M. Nedeljković, D. Veljković, S. D. Zarić, V. M. Rakić and I. A. Janković, *Phys. Chem. Chem. Phys.*, 2014, **16**, 20796–20805.
29 P. C. Redfern, P. Zapol, L. A. Curtiss, T. Rajh and M. C. Thurnauer, *J. Phys. Chem. B*, 2003, **107**, 11419–11427.
30 S. A. Mian, X. Gao, S. Nagase and J. Jang, *Theor. Chem. Acc.*, 2011, **130**, 333–339.
31 H. H. Kristoffersen, J. E. Shea and H. Metiu, *J. Phys. Chem. Lett.*, 2015, **6**, 2277–2281.
32 Y. Li, J. Wen, M. Qin, Y. Cao, H. Ma and W. Wang, *ACS Biomater. Sci. Eng.*, 2017, **3**, 979–989.
33 T. C. Genaro-Mattos, Â. Q. Maurício, D. Rettori, A. Alonso and M. Hermes-Lima, *PLoS One*, 2015, **10**(11), DOI: **10.1371/journal.pone.0129963**.
34 T. Kiss and A. Gergely, *Inorg. Chim. Acta*, 1979, **36**, 269–277.
35 D. Makovec, M. Komelj, G. Dražić, B. Belec, T. Goršak, S. Gyergyek and D. Lisjak, *Acta Mater.*, 2019, **172**, 84–91.
36 M. Lalia-Kantouri and Ch. Papadopoulos, *J. Therm. Anal. Calorim.*, 2005, **81**, 375–380.
37 G. Socrates, *Infrared and Raman Characteristic Group Frequencies*, John Wiley & Sons Ltd, Chichester, 2nd edn, 1994.
38 P. S. Pinto, G. D. Lanza, J. D. Ardisson and R. M. Lago, *J. Braz. Chem. Soc.*, 2019, **30**, 310–317.
39 T. Rajh, L. X. Chen, K. Lukas, T. Liu, M. C. Thurnauer and D. M. Tiede, *J. Phys. Chem. B*, 2002, **106**, 10543–10552.
40 IR Spectroscopy Tutorial: Carboxylic Acids, **https://orgchemboulder.com/Spectroscopy/irtutor/carbacidsir.shtml**, (accessed 3 October 2024).
41 J. Tosovic, *Kragujevac J. Sci*, 2017, 99–108.
42 R. Świsłocka, *Spectrochim. Acta, Part A*, 2013, **100**, 21–30.
43 G. L. Grice, E. Minogue, H. W. Coates, M. Debela, N. Kaneider-Kaser, P. R. Antrobus, R. S. Johnson and J. A. Nathan, ABHD11 mediated deglutarylation regulates the TCA cycle and T cell metabolism, *bioRxiV*, 2024, preprint, DOI: **10.1101/2024.09.11.612392**.
44 J. Coates, *Interpretation of Infrared Spectra, A Practical Approach*, Chichester, 2000.
45 Y. Hua, C. Wang, S. Wang and J. Xiao, *Environ. Sci. Pollut. Res.*, 2021, **28**, 62690–62702.
46 S. Zhang, S. Xu, Y. Liu, R. Lei, T. Guo, Y. Yao, S. Gao, J. Ding and Z. Zhang, *Prog. Nat. Sci.:Mater. Int.*, 2023, **33**, 37–46.
47 F. Gaboriaud and J.-J. Ehrhardt, *Geochim. Cosmochim. Acta*, 2003, 967–983.
48 A. J. A. Aquino, D. Tunega, G. Haberhauer, M. H. Gerzabek and H. Lischka, *Geochim. Cosmochim. Acta*, 2008, **72**, 3587–3602.
49 R. C. Plaza, J. L. Arias, M. Espín, M. L. Jiménez and A. V. Delgado, *J. Colloid Interface Sci.*, 2002, **245**, 86–90.
50 L. Čerović, G. Lefèvre, A. Jaubertie, M. Fédoroff and S. Milonjić, *J. Colloid Interface Sci.*, 2009, **330**, 284–291.
51 H. Hemmatpour, O. De Luca, D. Crestani, M. C. A. Stuart, A. Lasorsa, P. C. A. van der Wel, K. Loos, T. Giousis, V. Haddadi-Asl and P. Rudolf, *Nat. Commun.*, 2023, **14**, 664.
52 F. Gao, H. Qu, Y. Duan, J. Wang, X. Song, T. Ji, L. Cao, G. Nie and S. Sun, *RSC Adv.*, 2014, **4**, 6657–6663.
53 Y.-M. Chiang, D. P. Birnie and W. D. Kingery, *Physical Ceramics: Principles for Ceramic Science and Engineering*, Wiley, 1996.
54 G. Kaptay, *Int. J. Pharm.*, 2012, **430**, 253–257.
55 C. P. Huang, C. R. Chen, Y. F. Huang, Y. W. Lu and Y. H. Huang, *J. Mol. Catal. A:Chem.*, 2009, **304**, 121–127.
56 D. Lisjak, I. Arčon, M. Poberžnik, G. Herrero-Saboya, A. Tufani, A. Mavrič, M. Valant, P. H. Boštjančič, A. Mertelj, D. Makovec and L. Martin-Samos, *Sci. Rep.*, 2023, **13**, 1092.
57 R. H. Kodama, *Magn. Nanopart.*, 1999, **200**.
58 P. Guardia, B. Batlle-Brugal, A. G. Roca, O. Iglesias, M. P. Morales, C. J. Serna, A. Labarta and X. Batlle, *J. Magn. Magn. Mater.*, 2007, **316**, e756–e759.
59 C. R. Vestal and Z. J. Zhang, *J. Am. Chem. Soc.*, 2003, **125**, 9828–9833.